Eur. Phys. J. C 28, 525–533 (2003)
Digital Object Identifier (DOI) 10.1140/epjc/s2003-01191-7

THE EUROPEAN PHYSICAL JOURNAL C

# Coulomb interference in high-energy $pp$ and $\bar{p}p$ scattering

V.A. Petrov[1,a], E. Predazzi[2,b], A. Prokudin[1,2,c]

[1] Institute for High Energy Physics, 142281 Protvino, Russia
[2] Dipartimento di Fisica Teorica, Università Degli Studi Di Torino, Via Pietro Giuria 1, 10125 Torino, Italy and Sezione INFN di Torino, Italy

Received: 3 June 2002 / Revised version: 27 February 2003 /
Published online: 5 May 2003 – 

**Abstract.** An analysis of the Coulombic amplitude and its interference with the nuclear amplitude which is driven by the three-component pomeron is presented. It is shown that different approaches towards the evaluation of the Coulomb phase give approximately uniform results at all energies and the differences are negligible at RHIC and LHC energies. We show that the use of the amplitude which was fitted to accommodate the nucleon data only (in the region $0.01 \leq |t| \leq 14.5\,(\mathrm{GeV}^2)$), combined with the Coulomb amplitude, reproduces the existing data in the Coulomb interference domain quite accurately without any adjustment of the parameters. As a consequence, we predict the differential cross section in the region of the Coulomb nucleon interference for both RHIC and LHC energies.

## 1 Introduction

In [1] an eikonal model of a three-component pomeron has been suggested and successfully used for describing the high energy $pp$ and $\bar{p}p$ data in the region of large momentum transfer $0.01 \leq |t| \leq 14.5\,(\mathrm{GeV}^2)$. In this paper we apply this model to the region of small momentum transfer $0 \leq |t| \leq 0.01\,(\mathrm{GeV}^2)$.

The problem is a proper account of the Coulomb interaction which is most important at the smallest $|t|$. The standard way to do this is to represent the whole scattering amplitude $T(s,t)$ which is dominated by the Coulomb force at low momentum transfer and by the hadronic force at higher momentum transfer as

$$T(s,t) = T^{\mathrm{N}}(s,t) + \mathrm{e}^{\mathrm{i}\alpha\Phi} T^{\mathrm{C}}(s,t), \tag{1}$$

where, if we normalize the scattering amplitude so that

$$\frac{\mathrm{d}\sigma}{\mathrm{d}t} = \frac{|T(s,t)|^2}{16\pi s^2}, \tag{2}$$

the Born Coulomb amplitude for $pp$ and $\bar{p}p$ scattering is

$$T^{\mathrm{C}}(s,t) = \mp\frac{8\pi\alpha s}{|t|}. \tag{3}$$

The upper (lower) sign corresponds to the scattering of particles with the same (opposite) charges. $T^{\mathrm{N}}(s,t)$ stands for purely strong-interaction amplitude, and the phase $\Phi$ depends generally on energy, the momentum transfer and on the properties of $T^{\mathrm{N}}$. The study of the Coulomb–nuclear interference is very important for extracting the real part of the strong-interaction amplitude.

The issue of the Coulombic amplitude and its interference with the nuclear component was addressed in many papers in the past. West and Yennie [2] examined the Coulomb–nuclear interference using Feynman diagrams. Cahn [3] considered the same task in the framework of the eikonal model; his results were quite convincing (though the modifications were very small compared to [2]) and proved that the eikonal model is a very convenient basis for analyzing the Coulomb–nuclear interference. The role of the anomalous magnetic moment of the nucleon and its influence on the extraction of the $\rho$ values for $pp$ and $\bar{p}p$ scattering was addressed in [4].

The Coulombic phase has attracted the attention of many authors. Using the WKB approach in potential theory, Bethe [5] derived, for proton–nucleus scattering, the expression

$$\Phi = 2\ln(1.06/|\vec{k}_1|b\Theta), \tag{4}$$

where $|\vec{k}_1|$ is the c.m. momentum, $b$ is the range of the strong-interaction forces defined by the size of the nucleus, and $\Theta$ the c.m. scattering angle. Similar results were derived within potential theory by several authors [6,7].

A relativistic derivation of the phase was attempted by Soloviev [8], who obtained

$$\Phi = 2\ln(2/\Theta), \tag{5}$$

a result which differs considerably from the result of Bethe [5]. Utilizing the same technique, Rix and Thaler [9] derived a result quantitatively close to that of Bethe [5].

[a] e-mail: petrov@mx.ihep.su
[b] e-mail: predazzi@to.infn.it
[c] e-mail: prokudin@to.infn.it

West and Yennie [2], as already mentioned, obtained the phase of the Coulomb–nuclear interference using Feynman diagrams. For a conventional parametrization, $T^{\rm N}(s,t) \sim \exp(-B|t|/2)$, the result of West and Yennie [2] reads

$$\Phi_{\rm W-Y} = \mp\left[\ln(B|t|/2) + \gamma + O(B|t|)\right], \qquad (6)$$

where $\gamma = 0.577\cdots$ is Euler's constant. The upper (lower) sign corresponds to the scattering of $pp$ ($\bar{p}p$).

Cahn [3] analyzed also the effect of the electromagnetic form factor and obtained a general expression for the phase. The results of [3] were in complete agreement with [2] and especially the formula (6) was derived from a rather different perspective.

The main difference from the result [2] is a shift of the Coulomb amplitude due to the form factor's influence on the phase. If we introduce the electromagnetic form factor of the proton, the Born term of the Coulomb amplitude has the following form:

$$T^{\rm C}(s,t) = \mp\frac{8\pi\alpha s}{|t|} f^2(|t|), \qquad (7)$$

where the form factor may be chosen as

$$f(|t|) = {\rm e}^{-2|t|/\Lambda^2}, \;\; \Lambda^2 = 0.71\ {\rm GeV}^2. \qquad (8)$$

In this case the Coulomb phase has the following form:

$$\Phi_{Cahn} = \mp\left[\ln\left(\frac{B|t|}{2}\right) + \gamma + \ln\left(1+\frac{8}{B\Lambda^2}\right) + (4|t|/\Lambda^2)\ln(4|t|/\Lambda^2) + 2|t|/\Lambda^2\right]. \qquad (9)$$

All these results were obtained under the assumption that $|t| \to 0$. The derivation of the phase in a large domain of momentum transfer was attempted by Selyugin [10], and Kopeliovich and Tarasov [13]. In the region of interest for the present paper $0 \le |t| \le 0.01\,{\rm GeV}^2$, the latter results are similar to that of Cahn [3] and the main difference is in the dip region of the differential cross sections. The phase obtained in [10] accurately takes into account the dipole form factor

$$f(|t|) = \left[\frac{\Lambda^2}{\Lambda^2+|t|}\right]^2, \;\; \Lambda^2 = 0.71\,{\rm GeV}^2, \qquad (10)$$

and the complicated structure of the nucleon amplitude.

The phase has the following form:

$$\Phi_{\rm Selyugin} = \mp\left[\ln\frac{|t|}{4} + 2\gamma - \nu_s - {\rm i}\frac{8\pi s}{T_{\rm N}(s,t)}\int_0^\infty b{\rm d}bJ_0(b\sqrt{-t})\delta_{\rm C}(s,b) \times\left({\rm e}^{2{\rm i}\delta_{\rm N}(s,b)}-1\right)\right], \qquad (11)$$

where

$$\nu_s = 0.11\log(1+400|t|) \qquad (12)$$

takes into account the influence of the form factor on the pure Coulombic phase, and

$$\delta_{\rm C}(s,b) = \ln b + K_0(b\Lambda) + \frac{11}{12}b\Lambda K_1(b\Lambda) + \frac{5}{24}b^2\Lambda^2K_0(b\Lambda) + \frac{1}{48}b^3\Lambda^3K_1(b\Lambda). \qquad (13)$$

The prescription of West and Yennie [2] was successfully used by several authors [11,12] for describing differential cross sections in the low $t$ region.

In what follows we will investigate four different cases of the Coulomb phase – the phase calculated with the nucleon amplitude of the model [1] (which does not acquire any additional parameters) with the prescription of West and Yennie [2], the phase calculated with the prescription of Cahn [3], the prescription of Selyugin [10], and the phase equal to zero.

## 2 The nuclear amplitude

We believe that any nuclear amplitude that is capable of a high accuracy description of the combined set of high energy $pp$ and $\bar{p}p$ data (total and differential cross sections, $\rho$ parameter etc.) over the entire $|t|$ spectrum, if properly combined with the correct Coulomb amplitude *must* account well for the data in the interference region. That this is so we will prove using the particular nuclear amplitude which has been derived in [1] to describe the total and differential cross sections at high energies ($\sqrt{s} \ge 10\,{\rm GeV}$) in the range of momentum transfer $0.01 < |t| < 14.5\,{\rm GeV}^2$ using the eikonal approach (another one could have been the amplitude of [14]). We just write the nuclear amplitude of [1]

$$T(s,\vec{b}) = \frac{{\rm e}^{2{\rm i}\delta(s,\vec{b})}-1}{2{\rm i}}\,, \qquad (14)$$

where the eikonal has the following form:

$$\delta_{pp}^{\bar{p}p}(s,b) = \delta^+_{\mathbb{P}_1}(s,b) + \delta^+_{\mathbb{P}_2}(s,b) + \delta^+_{\mathbb{P}_3}(s,b) \mp \delta^-_{\mathbb{O}}(s,b) + \delta^+_f(s,b) \mp \delta^-_\omega(s,b). \qquad (15)$$

We refer the reader to the original literature for details; let us simply recall that here $\delta^+_{\mathbb{P}_{1,2,3}}(s,b)$ are pomeron contributions. The superscript "+" denotes $C$ even trajectories (the pomeron trajectories have quantum numbers $0^+J^{++}$), while "−" denotes $C$ odd trajectories. $\delta^-_{\mathbb{O}}(s,b)$ is the odderon contribution (i.e. the $C$ odd partner of the pomeron whose quantum numbers are $0^-J^{--}$); $\delta^+_f$ and $\delta^-_\omega(s,b)$ are the contributions of secondary reggeons ($f$ being a representative of the $C=+1$ families and $\omega$ of the $C=-1$ ones).

In order to relate $t$- and $b$-spaces one proceeds via Fourier–Bessel transforms:

$$\hat{f}(t) = 4\pi s\int_0^\infty {\rm d}b^2J_0(b\sqrt{-t})f(b)\,,$$
$$f(b) = \frac{1}{16\pi s}\int_{-\infty}^0 {\rm d}tJ_0(b\sqrt{-t})\hat{f}(t)\,. \qquad (16)$$

Using this parametrization we obtain the following expressions for the Coulomb phase:

$$\Phi_{\mathrm{W-Y}} = \mp \frac{\sum_i \delta_i(s,t=0)\left[\ln\left(\frac{\rho_i(s)|t|}{4}\right)+\gamma\right]}{\sum_i \delta_i(s,t=0)}, \qquad (17)$$

and

$$\Phi_{\mathrm{Cahn}} = \mp \frac{\sum_i \delta_i(s,t=0)\left[\ln\left(\frac{\rho_i(s)|t|}{4}\right)+\gamma+\ln\left(1+\frac{16}{\rho_i(s)A^2}\right)\right]}{\sum_i \delta_i(s,t=0)} \mp(4|t|/A^2)\ln(4|t|/A^2) \mp 2|t|/A^2, \qquad (18)$$

where $\rho_i^2 = 4\alpha_i'(0)\ln s/s_0 + r_i^2$, $i = P_1, P_2, P_3, O, f, \omega$. The upper (lower) signs correspond to $pp$ ($\bar{p}p$).

Crossing symmetry is restored by replacing $s \to s\mathrm{e}^{-\mathrm{i}\pi/2}$. We introduce the dimensionless variable

$$\tilde{s} = \frac{s}{s_0}\mathrm{e}^{-\mathrm{i}\frac{\pi}{2}}, \qquad (19)$$

in terms of which we give each $C+$ and $C-$ contribution with its appropriate signature factor in the form

$$\delta^+(s,b) = \mathrm{i}\frac{c}{s_0}\tilde{s}^{\alpha(0)-1}\frac{\mathrm{e}^{-\frac{b^2}{\rho^2}}}{4\pi\rho^2}, \quad \rho^2 = 4\alpha'(0)\ln\tilde{s} + r^2, \quad (C=+1); \qquad (20)$$

$$\delta^-(s,b) = \frac{c}{s_0}\tilde{s}^{\alpha(0)-1}\frac{\mathrm{e}^{-\frac{b^2}{\rho^2}}}{4\pi\rho^2}, \quad \rho^2 = 4\alpha'(0)\ln\tilde{s} + r^2, \quad (C=-1). \qquad (21)$$

One might imagine that a simple Gaussian form of the eikonal, (20), does not account for the complexity of the data, especially in the high $|t|$ region. Indeed in [1] we have found that an appropriate pomeron eikonal may be constructed as a sum of three terms, $\sum_{i=1,2,3}\delta_i^+(s,b)$, and the resulting amplitude gives a good agreement with the experimental data.

## 3 Results

In [1], the adjustable parameters have been fitted over a set of 982 $pp$ and $\bar{p}p$ data[1] of both forward observables (total cross sections $\sigma_{\mathrm{tot}}$, and the $\rho$, the ratios of real to imaginary parts of the amplitudes) in the range $8. \le \sqrt{s} \le 1800.\,\mathrm{GeV}$ and angular distributions ($\frac{\mathrm{d}\sigma}{\mathrm{d}t}$) in the ranges $23. \le \sqrt{s} \le 1800.\,\mathrm{GeV}$, $0.01 \le |t| \le 14.\,\mathrm{GeV}^2$. A good $\chi^2/\mathrm{d.o.f.} = 2.60$ was obtained and the parameters are given in Table 1.

**Table 1.** Parameters obtained in [1]

| | Pomeron$_1$ | | **f**-Reggeon |
|---|---|---|---|
| $\Delta_{\mathbb{P}_1}$ | $0.0578 \pm 0.0020$ | $\Delta_f$ | $-0.31$ (FIXED) |
| $c_{\mathbb{P}_1}$ | $53.007 \pm 0.795$ | $c_f$ | $191.69 \pm 2.12$ |
| $\alpha'_{\mathbb{P}_1}$ | $0.5596 \pm 0.0078\,(\mathrm{GeV}^{-2})$ | $\alpha'_f$ | $0.84\,(\mathrm{GeV}^{-2})$ (FIXED) |
| $r^2_{\mathbb{P}_1}$ | $6.3096 \pm 0.2522\,(\mathrm{GeV}^{-2})$ | $r_f^2$ | $31.593 \pm 1.099\,(\mathrm{GeV}^{-2})$ |
| | Pomeron$_2$ | | $\omega$-Reggeon |
| $\Delta_{\mathbb{P}_2}$ | $0.1669 \pm 0.0012$ | $\Delta_\omega$ | $-0.53$ (FIXED) |
| $c_{\mathbb{P}_2}$ | $9.6762 \pm 0.1600$ | $c_\omega$ | $-174.18 \pm 2.72$ |
| $\alpha'_{\mathbb{P}_2}$ | $0.2733 \pm 0.0056\,(\mathrm{GeV}^{-2})$ | $\alpha'_\omega$ | $0.93\,(\mathrm{GeV}^{-2})$ (FIXED) |
| $r^2_{\mathbb{P}_2}$ | $3.1097 \pm 0.1817\,(\mathrm{GeV}^{-2})$ | $r_\omega^2$ | $7.467 \pm 1.083\,(\mathrm{GeV}^{-2})$ |
| | Pomeron$_3$ | | |
| $\Delta_{\mathbb{P}_3}$ | $0.2032 \pm 0.0041$ | $s_0$ | $1.0\,(\mathrm{GeV}^2)$ (FIXED) |
| $c_{\mathbb{P}_3}$ | $1.6654 \pm 0.0669$ | | |
| $\alpha'_{\mathbb{P}_3}$ | $0.0937 \pm 0.0029\,(\mathrm{GeV}^{-2})$ | | |
| $r^2_{\mathbb{P}_3}$ | $2.4771 \pm 0.0964\,(\mathrm{GeV}^{-2})$ | | |
| | Odderon | | |
| $\Delta_{\mathbb{O}}$ | $0.19200 \pm 0.0025$ | | |
| $c_{\mathbb{O}}$ | $0.0166 \pm 0.0022$ | | |
| $\alpha'_{\mathbb{O}}$ | $0.048 \pm 0.0027\,(\mathrm{GeV}^{-2})$ | | |
| $r^2_{\mathbb{O}}$ | $0.1398 \pm 0.0570\,(\mathrm{GeV}^{-2})$ | | |

We now consider the complete set of data including the Coulomb region which consists of 2158 data[2]. To these data, we apply the model including the Coulomb part with its phase and we simply plot the physical quantities without any additional fitting.

The total cross sections and the ratios of real to imaginary parts of the forward amplitudes are presented in Figs. 1 and 2.

In order to compare the different approaches to the Coulomb phase, we have calculated the $\chi^2$ for the region of low $|t|$ : $0 \le |t| \le 0.01\,(\mathrm{GeV}^2)$ in four different cases:

(1) the Coulomb phase is equal to zero;
(2) the Coulomb phase is calculated with the prescription of West and Yennie (17);
(3) the Coulomb phase is calculated with the prescription of Cahn (18);
(4) the Coulomb phase is calculated with the prescription of Selyugin (11).

The results may be found in Table 2.

As is seen from Table 2, the experimental data marginally "prefer" the Coulomb phase calculated with the prescription of Cahn [3] and Selyugin [10] over that of

[1] The data are available at
REACTION DATA Database
http://durpdg.dur.ac.uk/hepdata/reac.html
CROSS SECTIONS PPDS database
http://wwwppds.ihep.su:8001/c5-5A.html
http://pdg.lbl.gov/2000/contents_plots.html

[2] The data are available at
REACTION DATA Database
http://durpdg.dur.ac.uk/hepdata/reac.html
CROSS SECTIONS PPDS database
http://wwwppds.ihep.su:8001/c5-5A.html
http://pdg.lbl.gov/2000/contents_plots.html

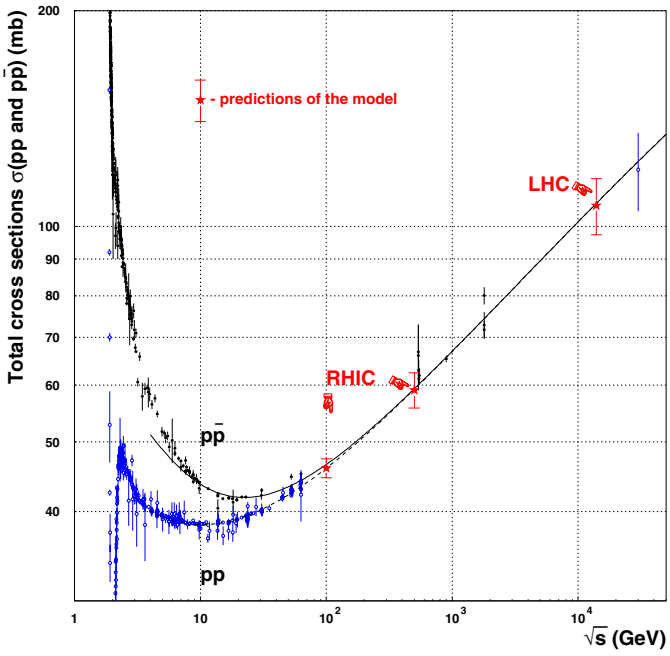


**Fig. 1.** Total cross sections of $pp$ scattering (*hollow circles*) and $\bar{p}p$ scattering (*full circles*) and corresponding curves in the model of [1]

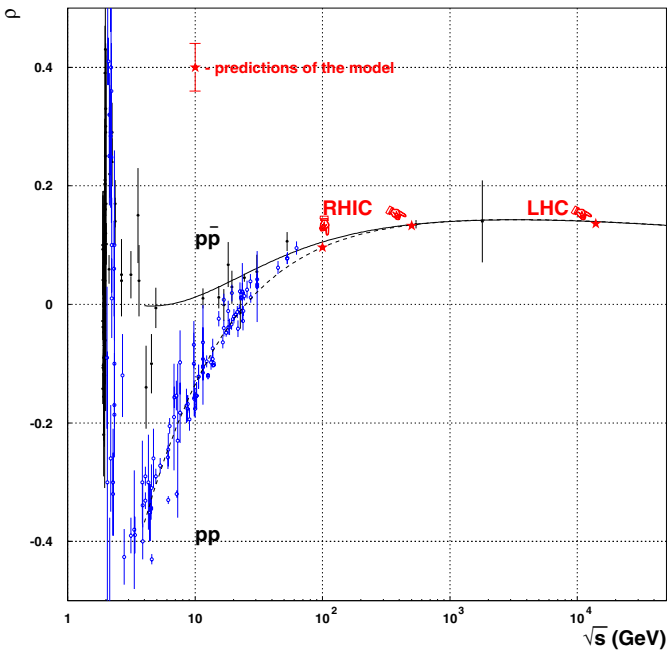


**Fig. 2.** Ratios of the real to the imaginary part of the forward $pp$ scattering amplitudes (*hollow circles*) and $\bar{p}p$ scattering amplitudes (*full circles*) and corresponding curves in the model of [1]

**Table 2.** $\chi^2$ per point for the region of low $|t|$ : $0 \le |t| \le 0.01\,(\mathrm{GeV}^2)$

| Coulomb phase | Number of points | $\chi^2$ per point |
|---|---|---|
| $\Phi = 0$ | 604 | 3.49 |
| $\Phi_{\mathrm{W-Y}}$ (17) | 604 | 2.09 |
| $\Phi_{\mathrm{Cahn}}$ (18) | 604 | 1.86 |
| $\Phi_{\mathrm{Selyugin}}$ (11) | 604 | 1.84 |

West and Yennie but taking the Coulomb phase equal to zero is excluded by the data and this is gratifying on physical grounds. The difference between the phases of [3] and [10] is negligible in the small $|t|$ region of interest (as may be seen in Fig. 3), though the exact result obtained in [10] over the whole kinematical region of $|t|$ shows that the difference is large in the region of the diffractive dip (as seen in Fig. 4).

Apart from this, the Coulomb phase calculated in the Selyugin approach exhibits a non-trivial behavior of the real part (which has a zero in the point of the diffractive dip), and of the imaginary part (which has a minimum in the same point); see Fig. 4.

The difference between the approaches of Cahn [3] and of West and Yennie [2] is more pronounced even in the region of low $t$ as may be seen in Fig. 3.

It is of some interest to perform a more detailed comparison of the $\chi^2$ derived for the region of low momentum transfer. This can be found in Table 3 for $\Phi_{\mathrm{W-Y}}$, $\Phi_{\mathrm{Cahn}}$, and $\Phi_{\mathrm{Selyugin}}$.

With all due caution, a general pattern emerges; some data points have anomalously large $\chi^2$ values and these are the same in all cases.

The $\bar{p}p$ differential cross section at $\sqrt{s} = 546\,\mathrm{GeV}$, for instance, sticks out conspicuously. The explanation is the normalization of the cross section. The systematical error allows us to change the normalization of the data in the $\pm 10\%$ corridor. If we could multiply our predictions by a factor 1.06, we would have a good description of this set of data, as is seen in Figs. 5 and 6.

To appreciate the role of the Coulomb phase, we plot the angular distributions with the appropriate Coulomb phase and with the phase taken equal to zero in Figs. 7 and 8. Even though the difference is minimal, the numerical conclusion is that the data, quite unambiguously, prefer the appropriate non-zero Coulomb phase.

The comparison with the West–Yennie and Cahn phases is not shown because the plot would be indistinguishable from the Selyugin one.

Let us recall that no additional fitting was done.

We do not report here any of the $pp$ and $\bar{p}p$ angular distributions which one obtains over the full range of $|t|$ values because the original reproduction of these quantities is left basically unchanged by the Coulomb amplitude and the interested reader is referred to the original paper [1]. We simply report here, for completeness, the predictions at RHIC and LHC energies both in the interference region and over the entire $|t|$ range. Predictions of the model and a comparison with the nuclear amplitude for RHIC and LHC are shown in Figs. 9, 10, 11 and 12.

To show the influence of the interference between nucleon and Coulomb amplitudes we show the ratio

$$R = \frac{\left| \frac{\mathrm{d}\sigma}{\mathrm{d}t} - \frac{\mathrm{d}\sigma_{\mathrm{nucleon}}}{\mathrm{d}t} - \frac{\mathrm{d}\sigma_{\mathrm{Coulomb}}}{\mathrm{d}t} \right|}{\frac{\mathrm{d}\sigma}{\mathrm{d}t}}\ [\%] \qquad (22)$$

**Table 3.** $\chi^2$ per point for the region of low $|t|$ : $0 \le |t| \le 0.01\,(\mathrm{GeV}^2)$ for $\Phi_{\mathrm{W-Y}}$, $\Phi_{\mathrm{Cahn}}$, and $\Phi_{\mathrm{Selyugin}}$

| | Data | $\sqrt{s}\,(\mathrm{GeV})$ | $0 \le \lvert t\rvert \le 0.01\,(\mathrm{GeV}^2)$ #points, ntot | $\chi^2$/ntot $\Phi_{\mathrm{W-Y}}$ | $\chi^2$/ntot $\Phi_{\mathrm{Cahn}}$ | $\chi^2$/ntot $\Phi_{\mathrm{Selyugin}}$ |
|---|---|---|---|---|---|---|
| 1 | $\sigma_{\mathrm{total}}^{\bar{p}p}$ | | 33 | 0.7167 | 0.7167 | 0.7167 |
| 2 | $\sigma_{\mathrm{total}}^{pp}$ | | 68 | 0.3617 | 0.3617 | 0.3617 |
| 3 | $\rho^{\bar{p}p}$ | | 11 | 0.6086 | 0.6086 | 0.6086 |
| 4 | $\rho^{pp}$ | | 48 | 0.4326 | 0.4326 | 0.4326 |
| 5 | $\frac{\mathrm{d}\sigma}{\mathrm{d}t}^{\bar{p}p}$ | 24.3 | 26 | 1.4965 | 2.4879 | 2.8105 |
| 6 | $\frac{\mathrm{d}\sigma}{\mathrm{d}t}^{\bar{p}p}$ | 30.4 | 21 | 1.4702 | 1.4130 | 1.4027 |
| 7 | $\frac{\mathrm{d}\sigma}{\mathrm{d}t}^{\bar{p}p}$ | 52.6 | 12 | 1.9847 | 1.4676 | 1.3440 |
| 8 | $\frac{\mathrm{d}\sigma}{\mathrm{d}t}^{\bar{p}p}$ | 62.3 | 3 | 1.0263 | 0.8135 | 0.7635 |
| 9 | $\frac{\mathrm{d}\sigma}{\mathrm{d}t}^{\bar{p}p}$ | 541.0 | 37 | 2.0811 | 2.3993 | 2.5246 |
| 10 | $\frac{\mathrm{d}\sigma}{\mathrm{d}t}^{\bar{p}p}$ | 546.0 | 15 | 11.4692 | 11.0364 | 10.9008 |
| 11 | $\frac{\mathrm{d}\sigma}{\mathrm{d}t}^{pp}$ | 10.6 | 35 | 2.3342 | 2.0297 | 1.9610 |
| 12 | $\frac{\mathrm{d}\sigma}{\mathrm{d}t}^{pp}$ | 12.3 | 37 | 1.5731 | 1.4169 | 1.3931 |
| 13 | $\frac{\mathrm{d}\sigma}{\mathrm{d}t}^{pp}$ | 19.4 | 45 | 1.9674 | 1.7840 | 1.7509 |
| 14 | $\frac{\mathrm{d}\sigma}{\mathrm{d}t}^{pp}$ | 22.2 | 45 | 1.4666 | 1.3374 | 1.3192 |
| 15 | $\frac{\mathrm{d}\sigma}{\mathrm{d}t}^{pp}$ | 23.9 | 94 | 2.3910 | 2.3699 | 2.3087 |
| 16 | $\frac{\mathrm{d}\sigma}{\mathrm{d}t}^{pp}$ | 24.3 | 25 | 1.1418 | 1.2638 | 1.3587 |
| 17 | $\frac{\mathrm{d}\sigma}{\mathrm{d}t}^{pp}$ | 27.4 | 40 | 2.2246 | 2.0014 | 1.9607 |
| 18 | $\frac{\mathrm{d}\sigma}{\mathrm{d}t}^{pp}$ | 30.7 | 8 | 0.3174 | 1.2071 | 1.5482 |
| 19 | $\frac{\mathrm{d}\sigma}{\mathrm{d}t}^{pp}$ | 44.7 | 25 | 5.0147 | 2.9964 | 2.7679 |
| 20 | $\frac{\mathrm{d}\sigma}{\mathrm{d}t}^{pp}$ | 52.8 | 21 | 7.1074 | 4.2590 | 3.9018 |
| 21 | $\frac{\mathrm{d}\sigma}{\mathrm{d}t}^{pp}$ | 62.3 | 4 | 8.5177 | 6.7054 | 6.2988 |

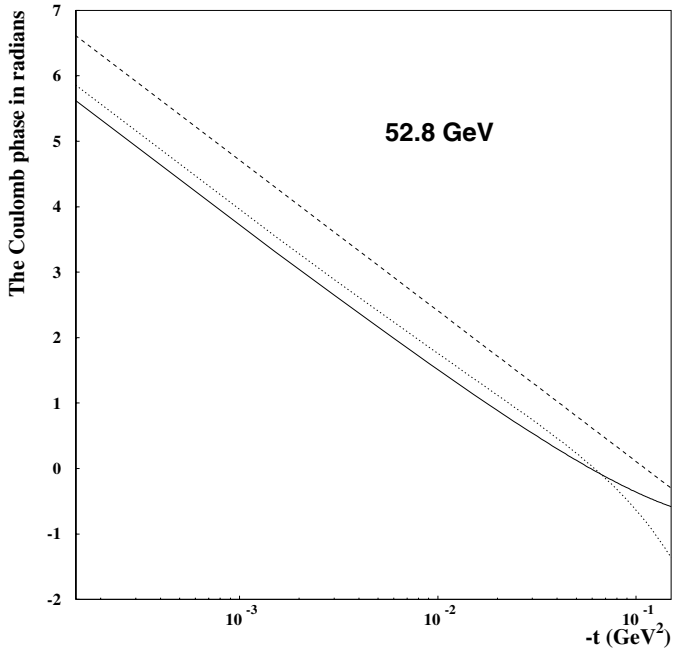


**Fig. 3.** The Coulomb phase calculated in the framework of Selyugin [10] (*solid line*) and of Cahn [3] (*dotted line*) and of West and Yennie [2] (*the dashed line*) in the region of small $t$. $\sqrt{s} = 52.8\,\mathrm{GeV}$

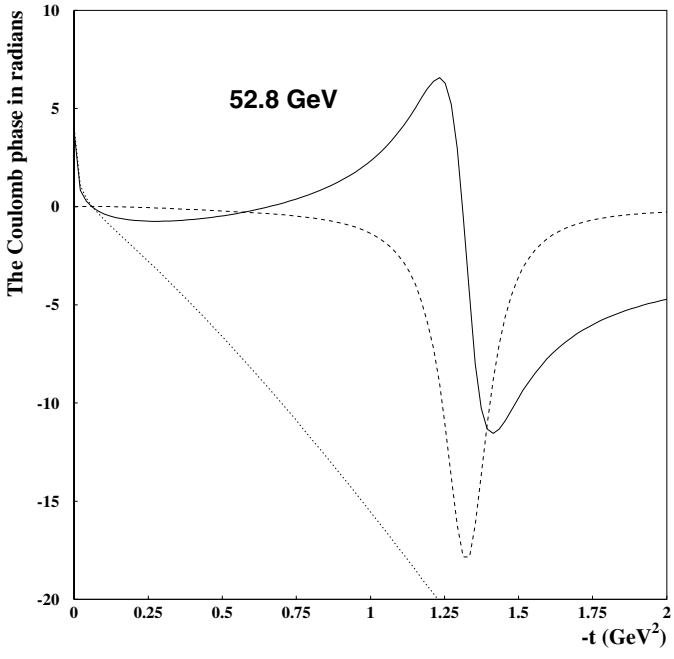


**Fig. 4.** The Coulomb phase calculated in the framework of Selyugin [10], real part (*solid line*) and imaginary part (*dashed line*) and in that of Cahn [3] (*dotted line*) in the region of high $t$

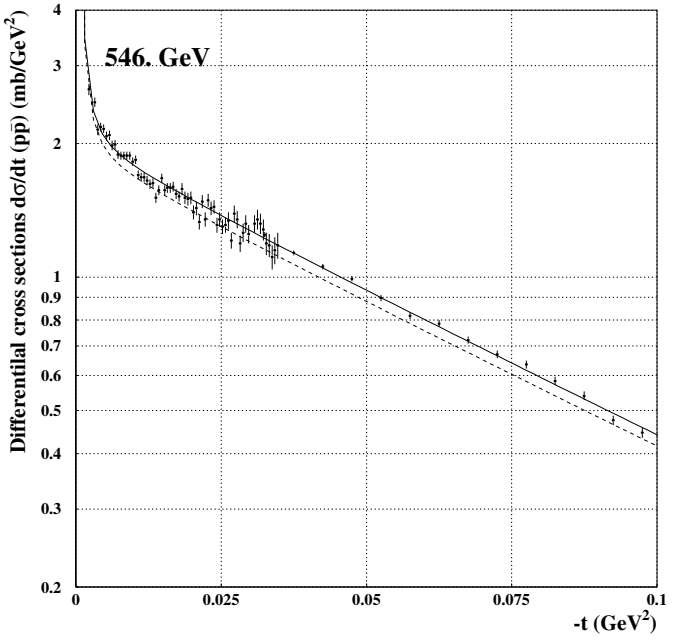


**Fig. 5.** Differential cross section of $\bar{p}p$ scattering and curves corresponding to its description in the model. The *dashed line* represents our predictions. The *solid curve* is our predictions normalized by a factor 1.06

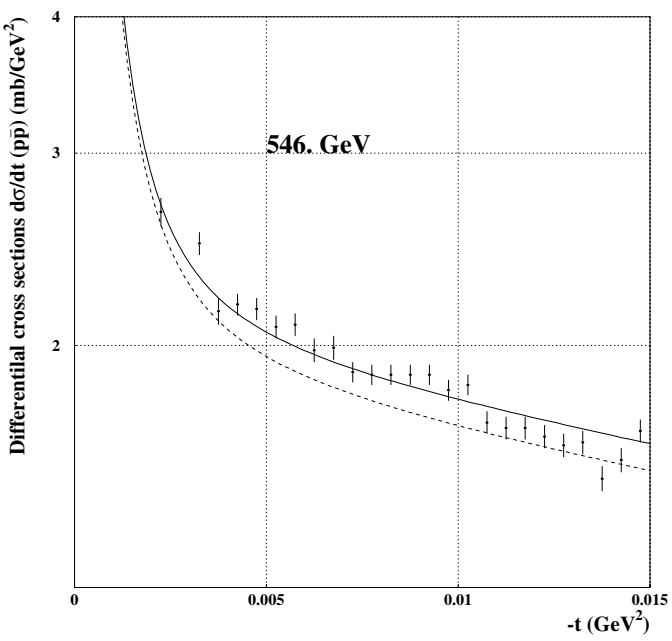


**Fig. 6.** The same as in Fig. 5 for low $t$

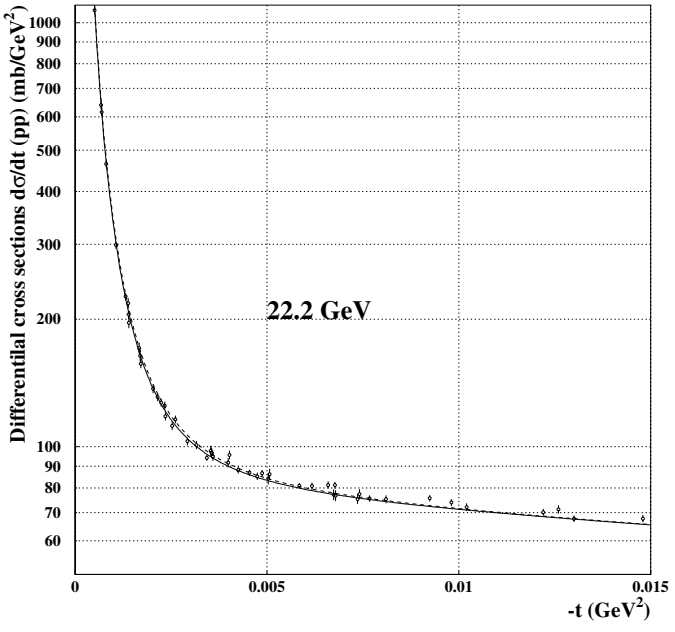


**Fig. 7.** Differential cross section of $pp$ scattering and curves corresponding to its description in the model. The *solid line* corresponds to the Coulomb phase calculated with the prescription of Selyugin (11) and the *dashed line* corresponds to the zero phase

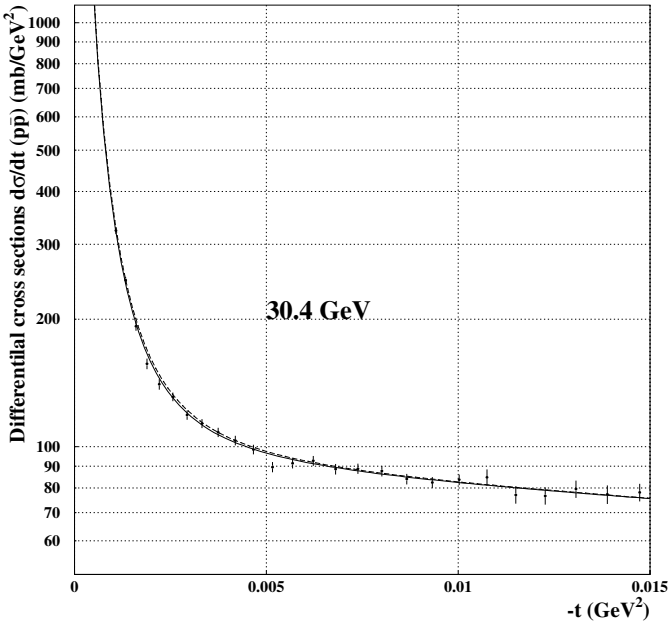


**Fig. 8.** Differential cross section of $\bar{p}p$ scattering and curves corresponding to its description in the model. The *solid line* corresponds to the Coulomb phase calculated with the prescription of Selyugin (11) and the *dashed line* corresponds to the zero phase

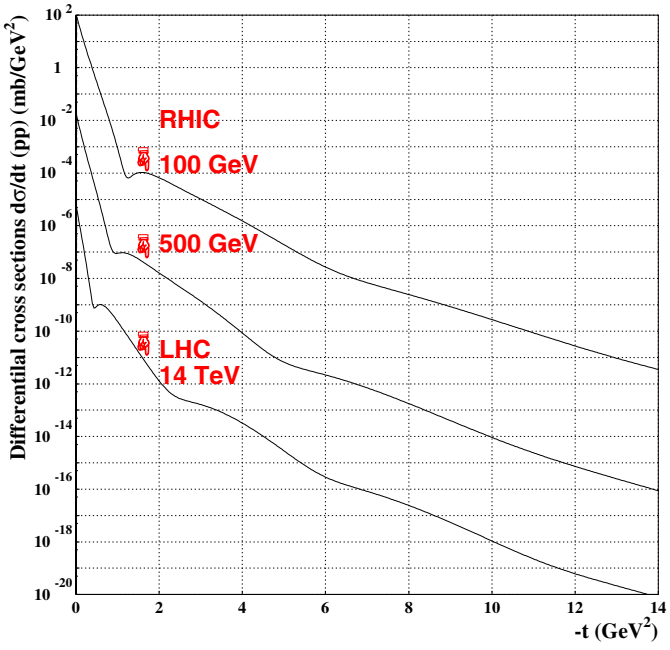


**Fig. 9.** Prediction of the model for the $pp$ scattering differential cross section at RHIC ($\sqrt{s} = 100,\ 500\,\text{GeV}$) and LHC ($\sqrt{s} = 14\,\text{TeV}$). A $10^{-4}$ factor between each successive set of data is omitted. The prediction for RHIC at the energy of $\sqrt{s} = 500\,\text{GeV}$ is multiplied by a factor of $10^{-4}$ and the prediction for LHC at the energy of $\sqrt{s} = 14\,\text{TeV}$ is multiplied by a factor of $10^{-8}$

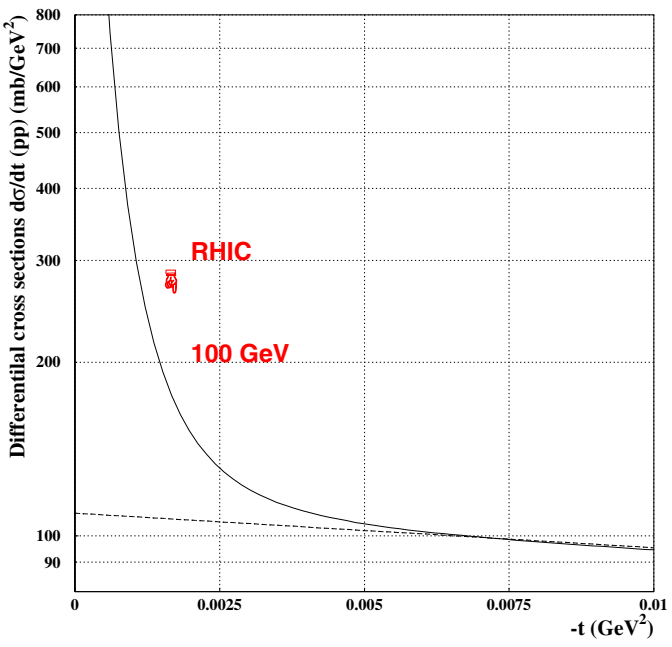


**Fig. 10.** Prediction of the model for the $pp$ scattering differential cross section at RHIC ($\sqrt{s} = 100\,\text{GeV}$). The *solid line* corresponds to the full amplitude including the Coulombic one and the *dashed line* corresponds to the nuclear amplitude [1]

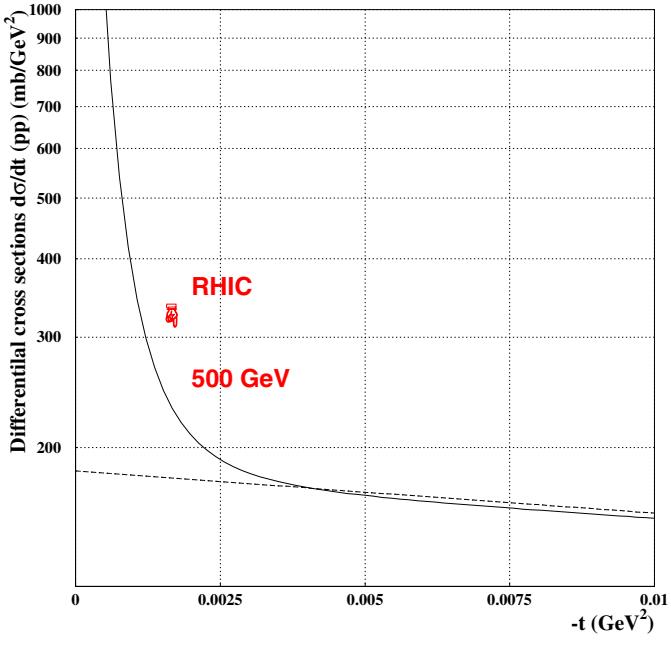


**Fig. 11.** Prediction of the model for the $pp$ scattering differential cross section at RHIC ($\sqrt{s} = 500\,\text{GeV}$). The *solid line* corresponds to the full amplitude including the Coulombic one and the *dashed line* corresponds to the nuclear amplitude [1]

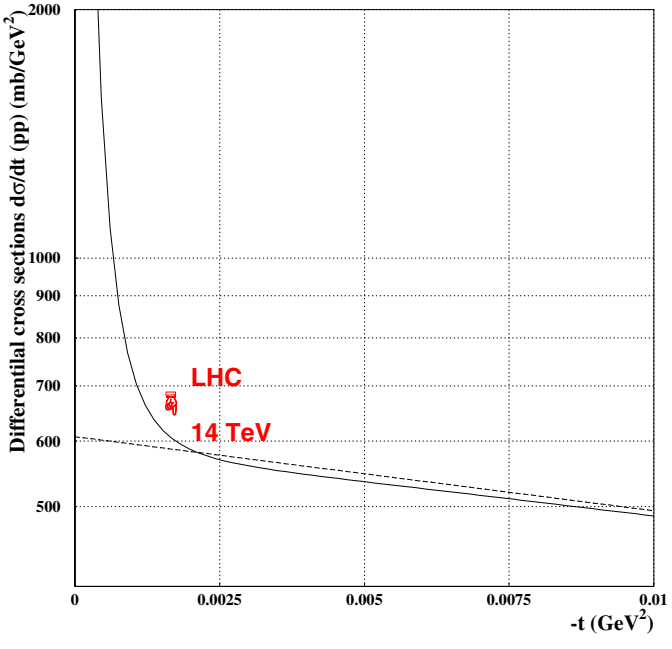


**Fig. 12.** Prediction of the model for the $pp$ scattering differential cross section at LHC ($\sqrt{s} = 14\,\text{TeV}$). The *solid line* corresponds to full amplitude including Coulombic one and the *dashed line* corresponds to the nuclear amplitude [1]

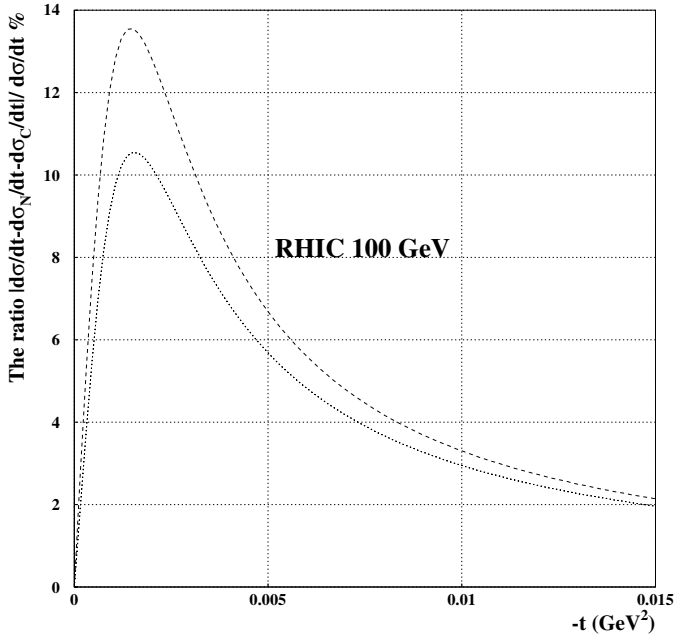


**Fig. 13.** The interference term between hadron and Coulomb amplitudes for at the RHIC energy. The *dashed line* corresponds to the Coulomb phase calculated with the prescription of Selyugin [10] and the *dotted line* to the zero Coulomb phase

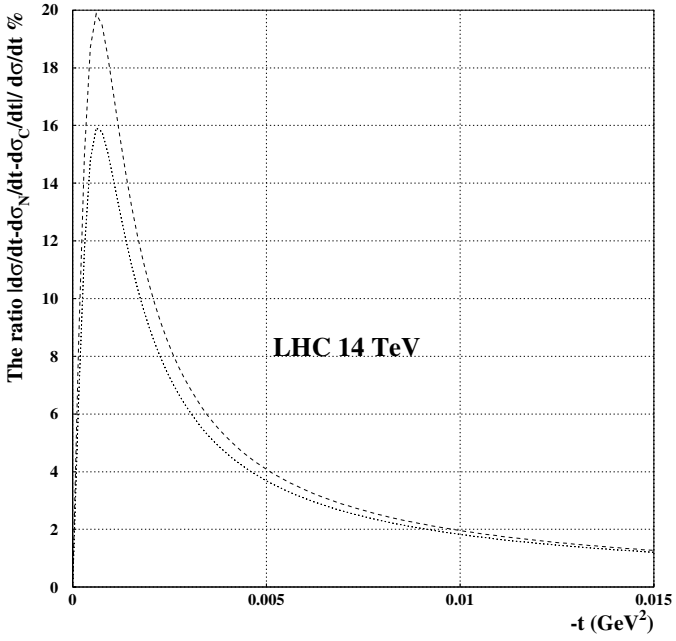


**Fig. 14.** The interference term between hadron and Coulomb amplitudes at the LHC energy. The *dashed line* corresponds to the Coulomb phase calculated with the prescription of Selyugin [10] and the *dotted line* to the zero Coulomb phase

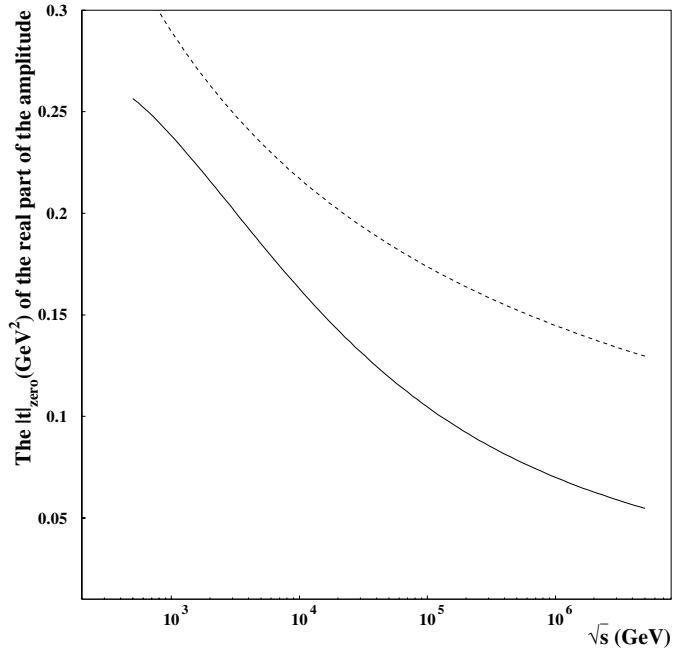


**Fig. 15.** The position of the zero of the real part of the scattering amplitude in a three-component pomeron model [1] (*solid line*) and in a "geometrical scaling" model $t_{\rm zero} = -1/(\lambda \ln s)$, $\lambda = 0.25\,\mathrm{GeV}^{-2}$ [15] (*dashed line*)

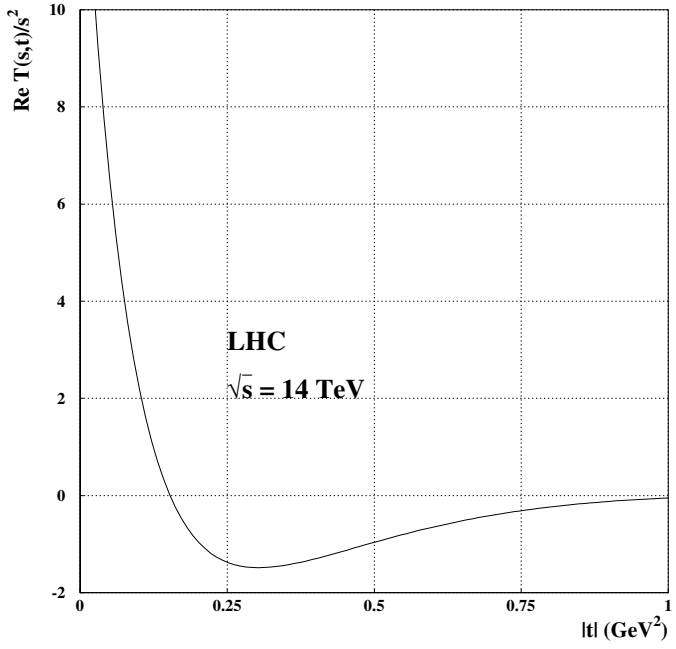


**Fig. 16.** The real part of the scattering amplitude at the LHC energy in the model of [1]

in Figs. 13 and 14 and we conclude that the interference term becomes negligible at RHIC and LHC energies at $t \sim -0.01\,\mathrm{GeV}^2$ for RHIC and $t \sim -0.005\,\mathrm{GeV}^2$ for LHC.

Now let us return to the problem of extracting the ratio $\rho(s, t = 0)$ of the real to the imaginary parts of the scattering amplitude. A general theorem [15] shows that this ratio as a function of the momentum transfer could not have a constant sign in a strip $s_M < s < \infty$, $-T < t \leq 0$, for any $s_M$ and $T > 0$. The method of extracting the ratio includes a simplification; the scattering amplitude is usually presented in the following form:

$$T(s,t) = \mp\frac{8\pi\alpha s}{|t|} f^2(|t|) + (\mathrm{i} + \rho(s,0)) s\sigma_{\mathrm{tot}} \mathrm{e}^{Bt}(1 - \mathrm{i}\alpha\Phi), \qquad (23)$$

where the ratio $\rho(s, t)$ is approximated by its value at $t = 0$. Should this simplification affect the measurement? The answer would be "yes" should the change of sign of $\rho$ occur close to the region of the maximum of the Coulomb nuclear interference.

In our particular model, the zero of the real part of the scattering amplitude goes to zero with the increase of energy, but remains far from the region of the maximum of the interference. For example, at LHC energies $\sqrt{s} = 14\,\mathrm{TeV}$, the maximum occurs at $|t_{\max}| \sim 10^{-3}\,\mathrm{GeV}^2$ (see Fig. 14) while the zero is at $|t_{\mathrm{zero}}| \sim 0.16\,\mathrm{GeV}^2$ (see Figs. 15 and 16), so the situation is not too bad.

## 4 Conclusion

All three choices for the Coulomb phase give a good description of the existing data; in terms of $\chi^2$ per point the phases calculated with the prescriptions of Cahn [3] (18) and Selyugin [10] (11) give us a slightly better $\chi^2$ (about 10% less than that of the phase calculated with the prescription of West and Yennie [2]). The experimental data, however, have a similar accuracy; therefore, we refrain from deriving the conclusion that the former phases are more accurate than the latter. We conclude that such prescriptions are a good basis for the evaluation of the Coulombic contribution in the full scattering amplitude. We expect that a similar conclusion would apply to an analysis repeated along the lines of [13], but we have not performed this analysis.

A further analysis of the problem, using other models for the hadronic amplitudes, might help to confirm our conclusions and to make them model independent.

As we have seen, the addition of the nuclear amplitude (with parameters fitted from total and differential cross sections) and of the Coulomb one (with its proper phase) is necessary to obtain a total amplitude which reproduces quite well the data in the interference region without any additional parameters and with no need to refit existing ones.

This allows us to predict the RHIC Coulomb interference which requires the measurements to start from $|t| \leq 0.005\,\mathrm{GeV}^2$ at the energy of $\sqrt{s} = 100\,\mathrm{GeV}$ and from $|t| \leq 0.004\,\mathrm{GeV}^2$ at the energy of $\sqrt{s} = 500\,\mathrm{GeV}$. Likewise, LHC will be able to cover the Coulomb region if the measurement starts from $|t| \leq 0.001\,\mathrm{GeV}^2$.

*Acknowledgements.* We would like to thank E. Martynov and O. Selyugin for useful discussions.

## References

1. V.A. Petrov, A.V. Prokudin, Eur. Phys. J. C **23**, 135 (2002)
2. G.B. West, D.R. Yennie, Phys. Rev. D **172**, 1413 (1968)
3. R. Cahn, Z. Phys. C **15**, 253 (1982)
4. M.M. Block, Phys. Rev. D **54**, 4337 (1996)
5. H. Bethe, Ann. Phys. **3**, 190 (1958)
6. J. Rix, R.M. Thaler, Phys. Rev. D **152**, 1357 (1966)
7. M.M. Islam, Phys. Rev. D **162**, 1426 (1967)
8. L.D. Soloviev, JETP **22**, 205 (1966)
9. J. Rix, R.M. Thaler, Phys. Rev. D **172**, 1414 (1968)
10. O.V. Selyugin, Phys. Rev. D **60**, 074028 (1999)
11. P. Desgrolard, A.I. Lengyel, E.S. Martynov, Nuovo Cimento A **110**, 251 (1997)
12. C. Bourelly, J. Soffer, Tai Tsun Wu, Z. Phys. C **37**, 369 (1988)
13. B.Z. Kopeliovich, A.V. Tarasov, Phys. Lett. B **497**, 44 (2001)
14. P. Desgrolard, M. Giffon, E. Martynov, E. Predazzi, Eur. Phys. J. C **16**, 499 (2000)
15. A. Martin, Phys. Lett. B **404**, 137 (1997)